

Fate of θ_{12} under $\mu - \tau$ Reflection Symmetry in Light of the First JUNO Results

Ranjeet Kumar[✉]

Institute for Convergence of Basic Studies, Seoul National University of Science and Technology, Seoul 01811, Republic of Korea

kumarranjeet.drk@gmail.com

The recent JUNO measurements of θ_{12} and Δm_{21}^2 open a new avenue for probing flavor symmetric structures in the lepton sector. Motivated by this, we study a model in which $\mu - \tau$ reflection symmetry naturally emerges from an underlying A_4 flavor symmetry within a type-II seesaw framework. Beyond its standard predictions of $\theta_{23} = 45^\circ$ and $\delta_{\text{CP}} = \pm\pi/2$, the framework yields testable predictions for θ_{12} that can be probed by JUNO. Two viable scenarios arise, one predicting $\sin^2 \theta_{12} \gtrsim 0.335$, which is strongly disfavored by the latest JUNO results. Correlations between θ_{12} and model parameters further enhance the model's predictivity. Future measurements at DUNE and T2HK will provide complementary tests of this scenario.

1. INTRODUCTION

The precision era of neutrino oscillation physics has been marked by substantial progress in probing lepton mixing parameters [1–8]. Recently, the next-generation Jiangmen Underground Neutrino Observatory (JUNO) has released its first measurements based on reactor antineutrino data [9–11]. With only 59.1 days of exposure, JUNO has already achieved unprecedented sensitivity to the solar oscillation parameters, $\sin^2 \theta_{12}$ and Δm_{21}^2 [12]. The reported best-fit values with 1σ uncertainties for the normal mass ordering scenario are

$$\sin^2 \theta_{12} = 0.3092 \pm 0.0087, \quad \Delta m_{21}^2 = (7.50 \pm 0.12) \times 10^{-5} \text{ eV}^2. \quad (1)$$

Even with its initial dataset, JUNO provides tighter constraints than current global fit analyses [13], further supported by independent reactor measurements from the SNO+ collaboration [14]. In turn, the solar sector is now strongly constrained, enabling more incisive tests of lepton mixing frameworks and placing tighter limits on viable flavor models [15–21]. Nonetheless, several fundamental questions remain to be addressed.

At present, the key unknowns in the neutrino oscillation sector are the neutrino mass ordering i.e., the sign of Δm_{31}^2 ($\Delta m_{31}^2 > 0$ corresponds to normal ordering and $\Delta m_{31}^2 < 0$

to inverted ordering), the octant of the atmospheric angle θ_{23} (lower octant if $\theta_{23} < 45^\circ$ and upper octant if $\theta_{23} > 45^\circ$), and the Dirac CP-violating phase δ_{CP} . The first JUNO results [12] already establish the foundation for its long term program to determine the neutrino mass ordering, while the remaining unknowns (θ_{23} and δ_{CP}) will be probed with high sensitivity by upcoming long-baseline experiments such as DUNE [22–24] and T2HK [25, 26]. The release of the first JUNO data have motivated a wide range of theoretical studies [27–36], including frameworks that predict nontrivial correlations among lepton mixing parameters [37–41]. Consequently, such scenarios are now being subject to increasingly stringent constraints from precision measurements in the solar sector.

In this context, we explore a flavor symmetric framework in which the precise JUNO measurements [12] play a decisive role, with further scrutiny expected from future long-baseline experiments [22–26]. We focus on a realization of $\mu - \tau$ reflection symmetry, which conventionally predicts a maximal atmospheric mixing angle, $\theta_{23} = 45^\circ$ and a maximal Dirac CP-violating phase, $\delta_{\text{CP}} = \pm\pi/2$ [42]. In its canonical formulation [43–54], the symmetry strictly fixes θ_{23} and δ_{CP} , while leaving the reactor mixing angle θ_{13} and solar mixing angle θ_{12} unconstrained, allowing them to take values consistent with experimental data. In the realization considered here, the framework further imposes a nontrivial constraint on θ_{12} , thereby enabling a direct confrontation with JUNO’s precision results [12].

In this work, the $\mu - \tau$ reflection symmetry naturally arises from an underlying A_4 flavor symmetry¹. Thanks to the A_4 structure [73], the framework establishes a predictive relation among the parameters, resulting in a constrained value of the solar mixing angle θ_{12} . The model is realized within a type-II seesaw mechanism [74–77] incorporating two types of $SU(2)_L$ triplet scalars, Δ and Δ' . The specific choice of the vacuum expectation value (vev) of these scalars gives rise to two different cases of $\mu - \tau$ reflection symmetry, each leading to distinctive constraints on the lepton mixing parameters. In light of the recent JUNO results [12], we focus here on the exact $\mu - \tau$ reflection symmetry scenario, which, in addition to the canonical predictions for θ_{23} and δ_{CP} , also constrains the solar mixing angle θ_{12} . Possible deviations from this exact scenario would result in a non-maximal θ_{23} and determine its octant. Such scenarios could be probed by upcoming experiments such as DUNE [22–24] and T2HK [25, 26], but they lie beyond the scope of the present study.

The structure of this paper is as follows. In Sec. 2, we outline the theoretical framework of the model based on A_4 flavor symmetry and discuss the emergence of a $\mu - \tau$ reflection symmetric neutrino mass matrix. In Sec. 3, we present the numerical results of the model, including possible correlations involving the mixing angle θ_{12} and examine their consistency with the recent JUNO results. Finally, we provide concluding remarks in Sec. 4.

¹ A number of selected studies based on A_4 in the literature can be found in Refs. [55–72].

2. MODEL FRAMEWORK

We consider a type-II seesaw model embedded within an A_4 flavor symmetry, in which $\mu - \tau$ reflection symmetry emerges naturally. Neutrino masses are generated via the type-II seesaw mechanism, and the A_4 symmetry governs the leptonic mixing pattern. We introduce two types of $SU(2)_L$ triplet scalars, Δ_i and Δ' , transforming as A_4 singlets $(1, 1'', 1')$ and a triplet (3) , respectively. The leptons L and l_{R_i} ($i = 1, 2, 3$) are assigned as 3 and $(1, 1'', 1')$ under A_4 , respectively. The Higgs-like doublets ϕ_α ($\alpha = e, \mu, \tau$), responsible for generating charged lepton masses, are assigned as triplets under A_4 . In addition, a discrete Z_3 symmetry is imposed to ensure that the charged lepton mass matrix remains diagonal, so that the leptonic mixing pattern is solely governed by the neutrino sector. Under the Z_3 symmetry, non-trivial charges are assigned exclusively to l_{R_i} and ϕ_α , whereas all other particles transform trivially. The particle content and their transformation properties under the various symmetries are summarized in Table I.

Fields	$SU(2)_L$	$U(1)_Y$	A_4	Z_3
L	2	$-1/2$	3	1
l_{R_i}	1	-1	$(1, 1'', 1')$	$(1, \omega^2, \omega)$
ϕ_α	2	$1/2$	$(3, 3, 3)$	$(1, \omega, \omega^2)$
Δ_i	3	1	$(1, 1'', 1')$	1
Δ'	3	1	3	1

TABLE I: Particle content and their transformation properties under different symmetries, where $i = 1, 2, 3$, and $\alpha = e, \mu, \tau$. To avoid confusion, the ω charge associated with the Z_3 symmetry is indicated in **boldface**, distinguishing it from the ω that appears in the A_4 tensor product rules (see App. A).

The transformations of Δ_i and Δ' are chosen such that their vev alignments $\langle \Delta_i \rangle = u_i$ and $\langle \Delta' \rangle = \frac{u'}{\sqrt{3}}(\pm 1, \omega, \omega^2)$ naturally realize the $\mu - \tau$ reflection symmetry. Depending on the sign choice in the vev alignment of Δ' , two distinct scenarios arise. Consequently, the model predicts the salient features of $\mu - \tau$ reflection symmetry, namely $\theta_{23} = 45^\circ$ and $\delta_{CP} = \pm\pi/2$. Beyond the standard $\mu - \tau$ reflection predictions, the structure imposed by the underlying A_4 symmetry tightly correlates the model parameters, resulting in robust and testable predictions for the solar mixing angle θ_{12} . Imposing neutrino oscillation constraints yields a lower bound on $\sin^2 \theta_{12}$ in one scenario, thereby enabling the latest JUNO results to probe this realization of the model. Having discussed the model framework, we next examine the generation of neutrino masses and the resulting mixing pattern.

2.1. Lagrangian and Neutrino Mass Matrix

Following the charge assignments of the particles under the various symmetries given in Table I, the invariant Yukawa Lagrangian that governs the leptonic sector can be formulated

as follows

$$\mathcal{L} = \mathcal{L}_\ell + \mathcal{L}_\nu, \quad (2)$$

where \mathcal{L}_ℓ is responsible for generating the charged lepton masses, and the neutrino masses can be extracted from \mathcal{L}_ν , given by

$$\begin{aligned} -\mathcal{L}_\ell &= y_e (\bar{L} \otimes \phi_e)_{\mathbf{1}} \otimes (l_{R_1})_{\mathbf{1}} + y_\mu (\bar{L} \otimes \phi_\mu)_{\mathbf{1}'} \otimes (l_{R_2})_{\mathbf{1}''} + y_\tau (\bar{L} \otimes \phi_\tau)_{\mathbf{1}''} \otimes (l_{R_3})_{\mathbf{1}'} + \text{h.c.}, \\ -\mathcal{L}_\nu &= \alpha_1 (\bar{L}^c \otimes L)_{\mathbf{1}} \otimes (i\tau_2 \Delta_1)_{\mathbf{1}} + \alpha_2 (\bar{L}^c \otimes L)_{\mathbf{1}'} \otimes (i\tau_2 \Delta_2)_{\mathbf{1}''} + \alpha_3 (\bar{L}^c \otimes L)_{\mathbf{1}''} \otimes (i\tau_2 \Delta_3)_{\mathbf{1}'} \\ &\quad + \beta (\bar{L}^c \otimes L)_{\mathbf{3S}} \otimes (i\tau_2 \Delta')_{\mathbf{3}} + \text{h.c.}, \end{aligned} \quad (3)$$

The lower indices in parentheses $[...]_p$; $p = 1, 1', 1'', 3_S, 3$ denote the A_4 transformation of enclosed fields. The vev alignments for ϕ_α are chosen as

$$\phi_e = v_1(1, 0, 0)^T, \quad \phi_\mu = v_2(0, 1, 0)^T, \quad \phi_\tau = v_3(0, 0, 1)^T. \quad (4)$$

This leads to a diagonal charged lepton mass matrix, implying that the leptonic mixing arises solely from the neutrino sector. We now rewrite \mathcal{L}_ν in its expanded form using the A_4 tensor product rules,

$$\begin{aligned} -\mathcal{L}_\nu &= \alpha_1 (\bar{L}_1^c L_1 + \bar{L}_2^c L_2 + \bar{L}_3^c L_3) i\tau_2 \Delta_1 + \alpha_2 (\bar{L}_1^c L_1 + \omega \bar{L}_2^c L_2 + \omega^2 \bar{L}_3^c L_3) i\tau_2 \Delta_2 \\ &\quad + \alpha_3 (\bar{L}_1^c L_1 + \omega^2 \bar{L}_2^c L_2 + \omega \bar{L}_3^c L_3) i\tau_2 \Delta_3 \\ &\quad + \beta [(\bar{L}_2^c L_3 + \bar{L}_3^c L_2) i\tau_2 \Delta'_a + (\bar{L}_3^c L_1 + \bar{L}_1^c L_3) i\tau_2 \Delta'_b + (\bar{L}_1^c L_2 + \bar{L}_2^c L_1) i\tau_2 \Delta'_c] + \text{h.c.} \end{aligned} \quad (5)$$

Here, the scalar Δ' , transforming as a triplet under A_4 , is defined as $\Delta' \equiv (\Delta'_a, \Delta'_b, \Delta'_c)^T$. Once the scalar fields Δ_i and Δ' acquire vevs, neutrino masses are generated. We adopt a specific vev alignments consistent with the minimization conditions of the scalar potential [78, 79], given by².

$$\langle \Delta_i \rangle = u_i, \quad \langle \Delta' \rangle = \frac{u'}{\sqrt{3}} (\pm 1, \omega, \omega^2)^T, \quad (6)$$

where $\omega^3 = 1$. Without loss of generality, we can consider the couplings α_i, β and vevs u_i, u' to be real. Thus, using Eqs. (5) and (6), the neutrino mass matrix can be extracted, which exhibits the $\mu - \tau$ reflection symmetric structure, given by

$$\mathcal{M}_\nu = \begin{pmatrix} A & C & C^* \\ C & B & D \\ C^* & D & B^* \end{pmatrix}, \quad (7)$$

² Another possible choice of vev alignment is $\langle \Delta' \rangle = \frac{u'}{\sqrt{3}} (\pm 1, \eta, \eta^{-1})^T$, where $\eta^2 = \omega$, which leads to identical predictions and is phenomenologically equivalent.

$$\text{where, } A = \sum_{i=1}^3 \alpha_i u_i, \quad B = \sum_{i=1}^3 \omega^{(2+i)} \alpha_i u_i, \quad D = \pm \frac{\beta u'}{\sqrt{3}}, \quad C = \omega^2 \frac{\beta u'}{\sqrt{3}} \equiv (\pm) D \omega^2. \quad (8)$$

The parameters A and D are real, whereas B and C are complex. As indicated in Eq. (8), the parameters C and D are not independent, leaving the model with only four effective free parameters.

3. NUMERICAL ANALYSIS AND MODEL PREDICTIONS

We now present a detailed numerical analysis of the model based on the neutrino mass matrix obtained in Eq. (7), which exhibits an exact $\mu - \tau$ reflection symmetry. Since the charged lepton mass matrix is diagonal, the leptonic mixing arises solely from the neutrino sector. As a consequence of the $\mu - \tau$ reflection symmetry, the atmospheric mixing angle and the Dirac CP-violating phase are fixed to $\theta_{23} = 45^\circ$ and $\delta_{\text{CP}} = \pm\pi/2$, respectively, independent of the specific values of the model parameters. In light of the recent JUNO results [12], we focus on observables that play a decisive role in testing the framework. In particular, the correlated behavior of the solar parameters $\sin^2 \theta_{12}$ and Δm_{21}^2 imposes strong constraints on the model.

We discuss two viable scenarios corresponding to the two possible vev alignments of the scalar Δ' . The associated vev alignments are: $\langle \Delta' \rangle \propto (1, \omega, \omega^2)^T$ and $\langle \Delta' \rangle \propto (-1, \omega, \omega^2)^T$, which lead to $D = +\beta \frac{u'}{\sqrt{3}}$ (case-I) and $D = -\beta \frac{u'}{\sqrt{3}}$ (case-II), respectively, in Eq. (7). The model involves four free parameters: two real parameters A and D , and one complex parameter B , parametrized as $B = r e^{i\theta}$. We carry out a parameter scan over the following ranges:

$$A = [10^{-4}, 10^{-1}], \quad |D| = [10^{-4}, 10^{-1}], \quad r = [10^{-4}, 10^{-1}], \quad \theta = [0, 2\pi], \quad (9)$$

For the numerical analysis, we impose the 3σ constraints on neutrino oscillation parameters from the AHEP global fit [80], given by

$$\begin{aligned} \Delta m_{21}^2 &= [6.94, 8.14] \times 10^{-5} \text{ eV}^2, & \Delta m_{31}^2 &= [2.47, 2.63] \times 10^{-3} \text{ eV}^2, \\ \sin^2 \theta_{12} &= [0.271, 0.369], & \sin^2 \theta_{13} &= [0.02000, 0.02405]. \end{aligned} \quad (10)$$

As noted above, the mixing angle θ_{23} is predicted to be 45° , which lies within the 3σ allowed range of AHEP global fit data.

We next present our model predictions for both scenarios mentioned above. The diagonalization procedure for the mass matrix in Eq. (7), together with the determination of the associated mixing angles, is outlined in App. B. We find that inverted ordering is disfavored in case-II, while case-I remains consistent with the current constraints. In the following, we focus on the normal ordering case, as it is the scenario probed by the recent JUNO measure-

ments. The solar mixing angle θ_{12} exhibits a robust correlation with the model parameters in both scenarios. For case-I, the predicted values of θ_{12} remain consistent with current data. In contrast, case-II predicts a lower bound on the solar mixing angle, $\sin^2 \theta_{12} \gtrsim 0.335$, which is nearly excluded at the 3σ level considering the JUNO results [12], although it remains compatible with the AHEP global fit data [80].

3.1. Constraints on Model Parameters from the Solar Mixing Angle θ_{12}

We begin by examining the correlation between the solar mixing angle θ_{12} and the model parameters. We find that $\sin^2 \theta_{12}$ exhibits a strong dependence on the ratios of model parameters, defined as $r_1 \equiv |D/A|$, $r_2 \equiv |D/B|$, and $r_3 \equiv |A/B| \equiv r_2/r_1$. The model predictions are shown as blue and green scatter points corresponding to case-I and case-II, respectively. In Fig. 1, we show the correlation between $\sin^2 \theta_{12}$ and the ratio r_1 . The left

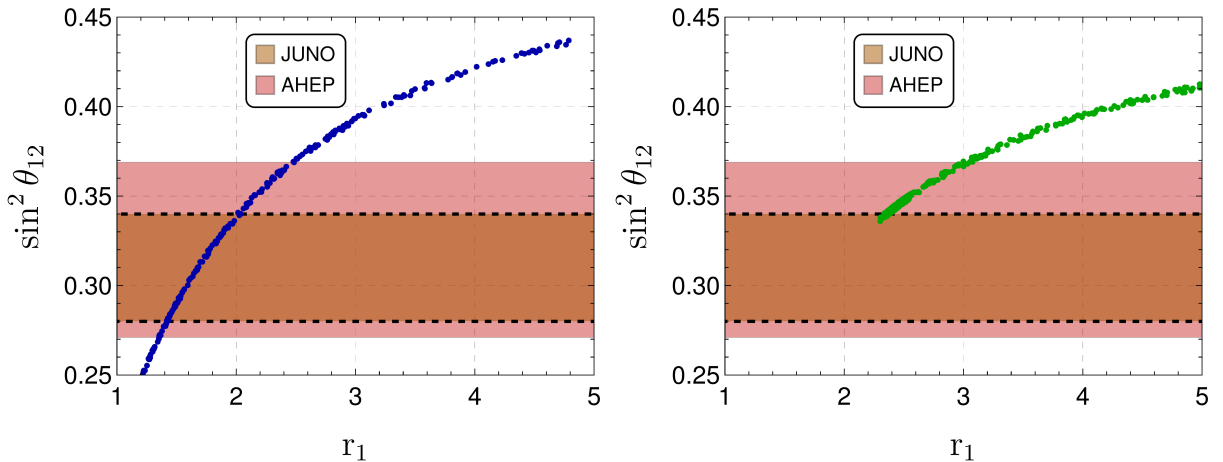


FIG. 1: Correlation between $\sin^2 \theta_{12}$ and the model parameter ratio r_1 . The predictions for case-I and case-II are shown in blue and green, respectively, in the left and right panels. The brown and light red bands represent the allowed 3σ ranges from JUNO and AHEP, respectively.

and right panels correspond to case-I and case-II, respectively. The allowed 3σ ranges of $\sin^2 \theta_{12}$ from JUNO and AHEP global fit are indicated by the brown and light red bands, respectively.

Similarly, we present the correlations for the ratios r_2 and r_3 in Figs. 2 and 3, respectively. The color code remains the same as in Fig. 1. The correlations observed in Figs. 1, 2, and 3 highlight the interplay between $\sin^2 \theta_{12}$ and the parameter ratios. In view of the recent JUNO measurement, these relations translate into stringent tests of the model. Once the mass-squared differences (Δm_{21}^2 and Δm_{31}^2) constraints are imposed, the free parameters of the model become correlated, leading to fixed ratios. The additional requirement of compatibility with $\sin^2 \theta_{12}$ further confines these ratios to a narrow region.

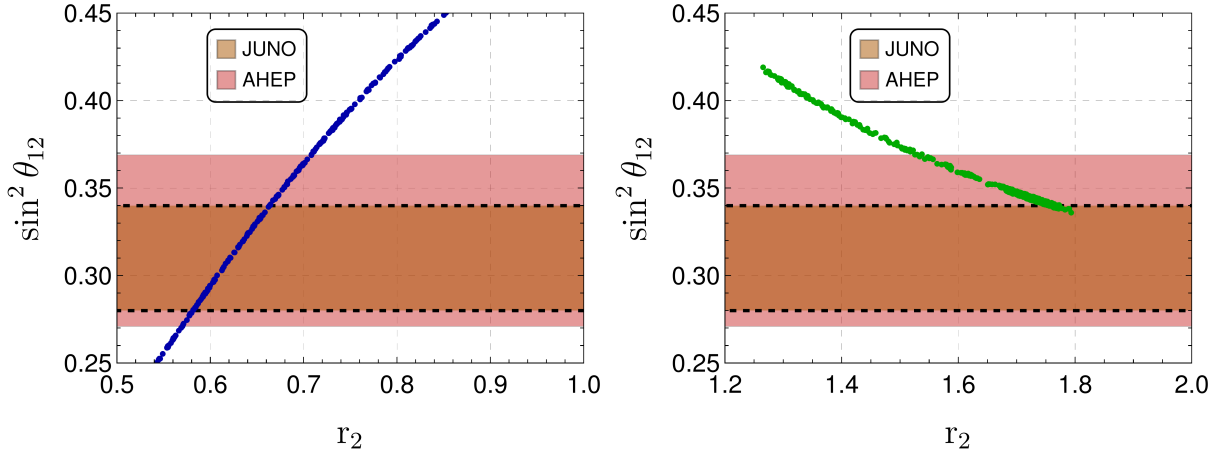


FIG. 2: Correlation between $\sin^2 \theta_{12}$ and the model parameter ratio r_2 . The color code remains the same as in Fig. 1.

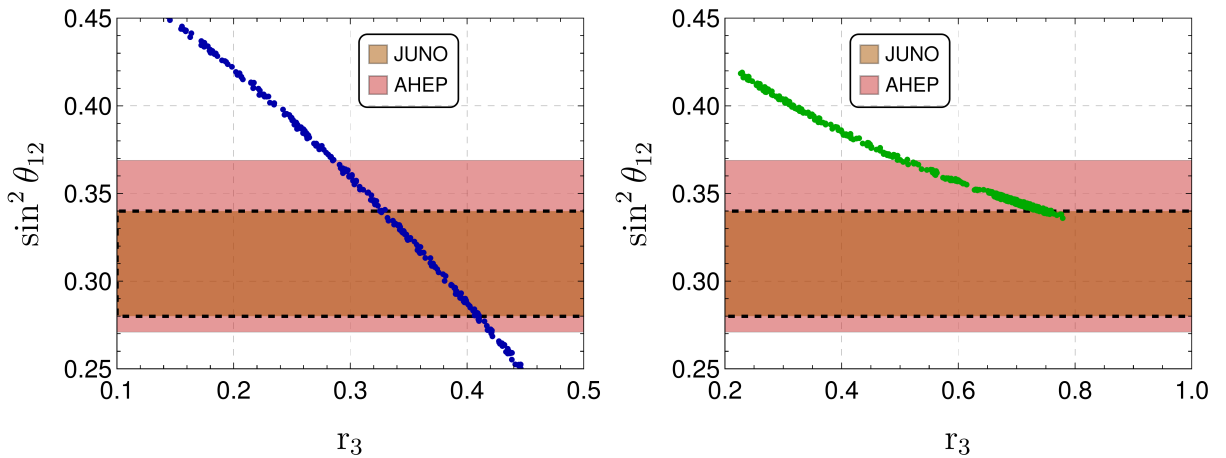


FIG. 3: Correlation between $\sin^2 \theta_{12}$ and the model parameter ratio r_3 . The color code remains the same as in Fig. 1.

In case-I, imposing the 3σ AHEP constraints confines the parameter ratios to the ranges: $r_1 \sim [1.3, 2.4]$, $r_2 \sim [0.57, 0.70]$, and $r_3 \sim [0.28, 0.42]$. While, for case-II the corresponding allowed ranges are: $r_1 \sim [2.4, 3.0]$, $r_2 \sim [1.5, 1.8]$, and $r_3 \sim [0.50, 0.78]$. In addition, case-II predicts a lower bound on the solar mixing angle, $\sin^2 \theta_{12} \gtrsim 0.335$. As a result, this scenario survives only within a very narrow region of the AHEP global fit parameter space and is almost excluded by the JUNO measurements. Notably, the origin of this constraint lies in the intrinsic correlation among the solar parameters, which we discuss next.

3.2. Solar Parameter Correlations in the Light of JUNO

We now turn to the correlation between the solar parameters $\sin^2 \theta_{12}$ and Δm_{21}^2 . The resulting predictions can be directly compared with the AHEP global fit data [80] and the

JUNO measurements [12]. Figure 4 illustrates the model correlations in the $(\sin^2 \theta_{12} - \Delta m_{21}^2)$ plane. The left panel represents the model predictions for case-I in blue, whereas the right panel shows the corresponding predictions for case-II in green. For the comparison, we

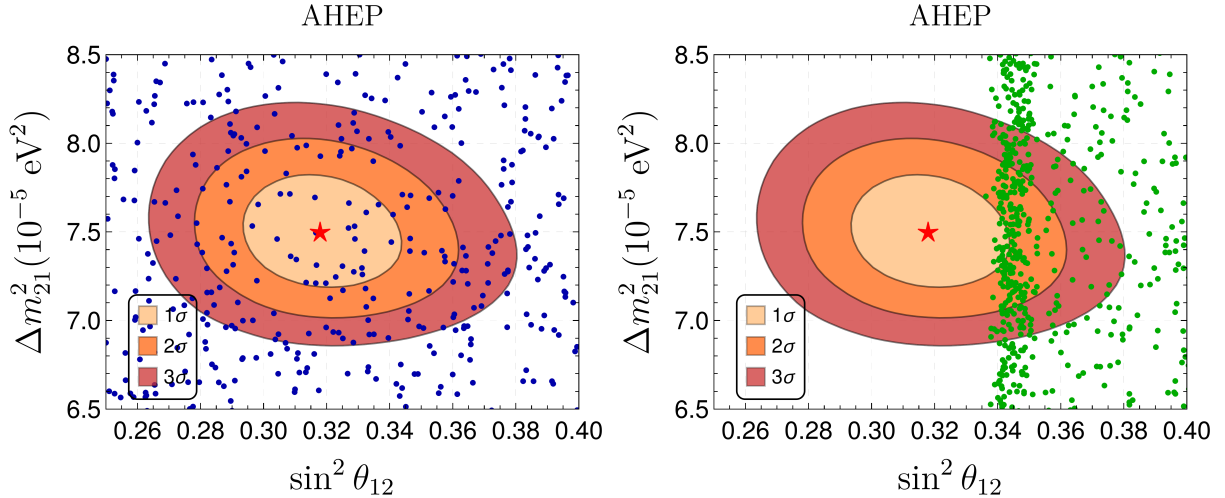


FIG. 4: Correlation between the solar parameters $\sin^2 \theta_{12}$ and Δm_{21}^2 predicted by the model, compared with the AHEP global fit data [80]. Case-I and case-II are shown in blue and green in the left and right panels, respectively.

consider the $1, 2, 3\sigma$ contours from the AHEP global fit in the $(\sin^2 \theta_{12} - \Delta m_{21}^2)$ plane, with the corresponding best-fit point indicated by a red star. After imposing the constraints from the reactor mixing angle θ_{13} and the atmospheric mass-squared difference Δm_{31}^2 , we find that the predictions of case-I, shown by blue points, span the entire allowed region. In contrast, the predictions of case-II, shown by green points, exhibit a lower bound on the solar mixing angle, $\sin^2 \theta_{12} \gtrsim 0.335$. Nevertheless, both scenarios remain compatible with the AHEP global fit data.

However, the presence of this lower bound in case-II suggests a restricted compatibility with the experimental data. This observation becomes particularly compelling considering the recent JUNO measurement of $\sin^2 \theta_{12}$. We therefore proceed to confront the model predictions with the JUNO data, which provide a more stringent and decisive test of the framework. The model predictions and their comparison with the $1, 2, 3\sigma$ contours of JUNO are shown in Fig. 5. The corresponding best-fit value is indicated by black star. As in Fig. 4, the left (right) panel corresponds to case-I (case-II). Since the blue points span the entire allowed region in the $(\Delta m_{21}^2 - \sin^2 \theta_{12})$ plane, case-I remains a viable scenario. In contrast, for case-II, the model predicts a lower bound $\sin^2 \theta_{12} \gtrsim 0.335$, causing all the green points to lie outside the 3σ JUNO contours. Consequently, in light of the JUNO results, this scenario of the model is nearly excluded.

Therefore, by comparing Figs. 4 and 5, we observe that prior to the JUNO measurements, case-II was also consistent and remained well within the 2σ range of the AHEP global fit data. However, once the JUNO results are taken into account, only the first scenario, case-I

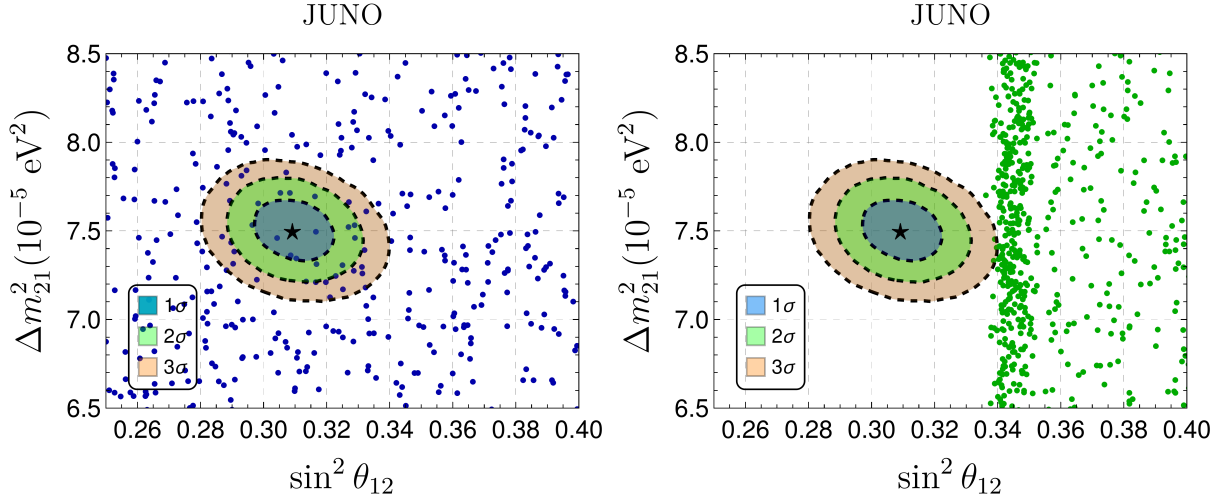


FIG. 5: Correlation between the solar parameters $\sin^2 \theta_{12}$ and Δm_{21}^2 predicted by the model, compared with the JUNO results [80]. Case-I and case-II are shown in blue and green in the left and right panels, respectively.

$(D = +\beta \frac{u'}{\sqrt{3}})$, remains compatible, while the second one $(D = -\beta \frac{u'}{\sqrt{3}})$ is almost ruled out.

4. CONCLUSIONS

We have developed a framework in which $\mu - \tau$ reflection symmetry is naturally realized as a consequence of an underlying A_4 flavor symmetry. Neutrino masses are generated via the type-II seesaw mechanism through the introduction of two $SU(2)_L$ triplet scalars: Δ_i and Δ' , transforming as singlets and a triplet under A_4 , respectively. The specific vev alignments of these scalars lead to an exact $\mu - \tau$ reflection symmetry in the neutrino sector. Depending on the choice of vev alignment for Δ' , two distinct viable scenarios emerge. An additional Z_3 symmetry ensures a diagonal charged lepton mass matrix, leaving the leptonic mixing entirely governed by the neutrino sector. The resulting $\mu - \tau$ reflection symmetry then fixes the atmospheric mixing angle to $\theta_{23} = 45^\circ$ and the Dirac CP-violating phase to $\delta_{\text{CP}} = \pm\pi/2$.

Beyond the well known predictions arising from $\mu - \tau$ reflection symmetry, our framework yields nontrivial and testable implications for the solar mixing angle θ_{12} . In particular, when combined with the solar mass-squared difference Δm_{21}^2 , the model predictions can be directly confronted with the latest JUNO measurements. Among the two distinct scenarios, one predicts $\sin^2 \theta_{12} \gtrsim 0.335$, which is strongly disfavored by the JUNO results, although it remains compatible with the current AHEP global fit data. In both cases, $\sin^2 \theta_{12}$ exhibits a robust correlation with the ratios of the underlying model parameters. Imposing the neutrino oscillation constraints significantly narrows the allowed range of these ratios, thereby reducing the parametric freedom of the model and enhancing its phenomenological implications.

Furthermore, future measurements of the θ_{23} octant at DUNE and T2HK will play an

important role in probing extensions of this framework that introduce controlled deviations from exact $\mu - \tau$ reflection symmetry. The observation of a non-maximal θ_{23} with a specific octant preference would provide compelling evidence in favor of such scenarios.

ACKNOWLEDGMENTS

RK would like to acknowledge support from the National Research Foundation of Korea under grant NRF-2023R1A2C100609111.

Appendix A: Tensor Product Rules of A_4

The A_4 symmetry is a non-abelian discrete flavor group. It corresponds to the group of even permutations of four objects and is isomorphic to the symmetry group of a regular tetrahedron. The group contains 12 elements and can be generated by two generators S and T obeying the relations:

$$S^2 = T^3 = (ST)^3 = I. \quad (\text{A1})$$

In the basis where S and T are real matrices, the generators are given by,

$$S = \begin{pmatrix} 1 & 0 & 0 \\ 0 & -1 & 0 \\ 0 & 0 & -1 \end{pmatrix}, \quad T = \begin{pmatrix} 0 & 1 & 0 \\ 0 & 0 & 1 \\ 1 & 0 & 0 \end{pmatrix}. \quad (\text{A2})$$

The A_4 group has four irreducible representations, three of them are one dimensional (i.e., three singlets) 1 , $1'$, and $1''$, and one of them is three dimensional (triplet) 3 . The multiplication rules for these representations are given as follows:

$$\begin{aligned} 1 \times 1 &= 1 = 1' \times 1'', \quad 1' \times 1' = 1'', \quad 1'' \times 1'' = 1', \\ 1 \times 3 &= 3, \quad 3 \times 3 = 1 + 1' + 1'' + 3_S + 3_A. \end{aligned} \quad (\text{A3})$$

where 3_S and 3_A denote the two independent triplet contractions arising from the product of two triplets. If $a = (a_1, a_2, a_3)$ and $b = (b_1, b_2, b_3)$ are two triplets then their multiplication rules are constructed as follows [73]:

$$\begin{aligned} (ab)_1 &= a_1b_1 + a_2b_2 + a_3b_3, \\ (ab)_{1'} &= a_1b_1 + \omega a_2b_2 + \omega^2 a_3b_3, \\ (ab)_{1''} &= a_1b_1 + \omega^2 a_2b_2 + \omega a_3b_3, \\ (ab)_{3_S} &= (a_2b_3 + a_3b_2, a_3b_1 + a_1b_3, a_1b_2 + a_2b_1)^T, \\ (ab)_{3_A} &= (a_2b_3 - a_3b_2, a_3b_1 - a_1b_3, a_1b_2 - a_2b_1)^T, \end{aligned} \quad (\text{A4})$$

where ω is the cube root of unity defined by $\omega = e^{2\pi i/3}$. The triplets 3_S and 3_A denotes the symmetric and antisymmetric contractions, respectively.

Appendix B: Determination of Lepton Mixing Parameters

The neutrino mass matrix given in Eq. (7) can be diagonalized by a unitary transformation as follows

$$U_\nu^T \mathcal{M}_\nu U_\nu = \text{diag}(m_1, m_2, m_3), \quad (\text{B1})$$

where U_ν is the unitary matrix and $m_{1,2,3}$ denote the physical neutrino mass eigenvalues. In the present framework, the charged lepton mass matrix is diagonal. Consequently, U_ν directly corresponds to the leptonic mixing (PMNS) matrix,

$$U_{\text{PMNS}} \equiv U_\nu. \quad (\text{B2})$$

We choose the symmetric parametrization of the lepton mixing matrix [74, 81], given by

$$U_{\text{PMNS}} = P(\delta_1, \delta_2, \delta_3) U_{23}(\theta_{23}, \phi_{23}) U_{13}(\theta_{13}, \phi_{13}) U_{12}(\theta_{12}, \phi_{12}), \quad (\text{B3})$$

where $P(\delta_1, \delta_2, \delta_3)$ is a diagonal matrix of unphysical phases and the U_{ij} are complex rotations in the ij plane, as for example,

$$U_{23}(\theta_{23}, \phi_{23}) = \begin{pmatrix} 1 & 0 & 0 \\ 0 & \cos \theta_{23} & \sin \theta_{23} e^{-i\phi_{23}} \\ 0 & -\sin \theta_{23} e^{i\phi_{23}} & \cos \theta_{23} \end{pmatrix}. \quad (\text{B4})$$

The phases ϕ_{12} and ϕ_{13} are relevant for neutrinoless double beta decay, while the combination $\delta_{CP} = \phi_{13} - \phi_{12} - \phi_{23}$ is the usual Dirac CP-violating phase measured in neutrino oscillations. The leptonic mixing angles can be extracted from the elements of the PMNS matrix through the following relations:

$$s_{13} = |U_{\text{PMNS}}|_{13}, \quad s_{12} = |U_{\text{PMNS}}|_{12}/c_{13}, \quad s_{23} = |U_{\text{PMNS}}|_{23}/c_{13}. \quad (\text{B5})$$

where $s_{13,12,23}$ and c_{13} denote the shorthand notations for $\sin \theta_{13,12,23}$ and $\cos \theta_{13}$, respectively.

[1] **Kamiokande-II** Collaboration, K. S. Hirata *et al.*, “Results from one thousand days of real

time directional solar neutrino data,” *Phys. Rev. Lett.* **65** (1990) 1297–1300.

[2] **Kamiokande-II** Collaboration, K. S. Hirata *et al.*, “Observation of a small atmospheric muon-neutrino / electron-neutrino ratio in Kamiokande,” *Phys. Lett. B* **280** (1992) 146–152.

[3] **Super-Kamiokande** Collaboration, Y. Fukuda *et al.*, “Evidence for oscillation of atmospheric neutrinos,” *Phys. Rev. Lett.* **81** (1998) 1562–1567, [arXiv:hep-ex/9807003](https://arxiv.org/abs/hep-ex/9807003).

[4] B. T. Cleveland, T. Daily, R. Davis, Jr., J. R. Distel, K. Lande, C. K. Lee, P. S. Wildenhain, and J. Ullman, “Measurement of the solar electron neutrino flux with the Homestake chlorine detector,” *Astrophys. J.* **496** (1998) 505–526.

[5] **SNO** Collaboration, Q. R. Ahmad *et al.*, “Direct evidence for neutrino flavor transformation from neutral current interactions in the Sudbury Neutrino Observatory,” *Phys. Rev. Lett.* **89** (2002) 011301, [arXiv:nucl-ex/0204008](https://arxiv.org/abs/nucl-ex/0204008).

[6] **Double Chooz** Collaboration, Y. Abe *et al.*, “Indication of Reactor $\bar{\nu}_e$ Disappearance in the Double Chooz Experiment,” *Phys. Rev. Lett.* **108** (2012) 131801, [arXiv:1112.6353](https://arxiv.org/abs/1112.6353) [hep-ex].

[7] **Daya Bay** Collaboration, F. P. An *et al.*, “Observation of electron-antineutrino disappearance at Daya Bay,” *Phys. Rev. Lett.* **108** (2012) 171803, [arXiv:1203.1669](https://arxiv.org/abs/1203.1669) [hep-ex].

[8] **RENO** Collaboration, J. K. Ahn *et al.*, “Observation of Reactor Electron Antineutrino Disappearance in the RENO Experiment,” *Phys. Rev. Lett.* **108** (2012) 191802, [arXiv:1204.0626](https://arxiv.org/abs/1204.0626) [hep-ex].

[9] **JUNO** Collaboration, A. Abusleme *et al.*, “JUNO physics and detector,” *Prog. Part. Nucl. Phys.* **123** (2022) 103927, [arXiv:2104.02565](https://arxiv.org/abs/2104.02565) [hep-ex].

[10] **JUNO** Collaboration, A. Abusleme *et al.*, “Sub-percent precision measurement of neutrino oscillation parameters with JUNO,” *Chin. Phys. C* **46** no. 12, (2022) 123001, [arXiv:2204.13249](https://arxiv.org/abs/2204.13249) [hep-ex].

[11] **JUNO** Collaboration, A. Abusleme *et al.*, “Potential to identify neutrino mass ordering with reactor antineutrinos at JUNO,” *Chin. Phys. C* **49** no. 3, (2025) 033104, [arXiv:2405.18008](https://arxiv.org/abs/2405.18008) [hep-ex].

[12] **JUNO** Collaboration, A. Abusleme *et al.*, “First measurement of reactor neutrino oscillations at JUNO,” [arXiv:2511.14593](https://arxiv.org/abs/2511.14593) [hep-ex].

[13] **Particle Data Group and 2025 update** Collaboration, S. Navas *et al.*, “Review of particle physics,” *Phys. Rev. D* **110** no. 3, (2024) 030001.

[14] **SNO+** Collaboration, M. Abreu *et al.*, “Measurement of reactor antineutrino oscillations with 1.46 ktonne-years of data at SNO+,” [arXiv:2511.11856](https://arxiv.org/abs/2511.11856) [hep-ex].

[15] S. F. King, “Unified Models of Neutrinos, Flavour and CP Violation,” *Prog. Part. Nucl. Phys.* **94** (2017) 217–256, [arXiv:1701.04413](https://arxiv.org/abs/1701.04413) [hep-ph].

[16] F. Feruglio and A. Romanino, “Lepton flavor symmetries,” *Rev. Mod. Phys.* **93** no. 1, (2021) 015007, [arXiv:1912.06028](https://arxiv.org/abs/1912.06028) [hep-ph].

- [17] Z.-z. Xing, “Flavor structures of charged fermions and massive neutrinos,” *Phys. Rept.* **854** (2020) 1–147, [arXiv:1909.09610 \[hep-ph\]](https://arxiv.org/abs/1909.09610).
- [18] Y. Almumin, M.-C. Chen, M. Cheng, V. Knapp-Perez, Y. Li, A. Mondol, S. Ramos-Sanchez, M. Ratz, and S. Shukla, “Neutrino Flavor Model Building and the Origins of Flavor and CP Violation,” *Universe* **9** no. 12, (2023) 512, [arXiv:2204.08668 \[hep-ph\]](https://arxiv.org/abs/2204.08668).
- [19] G. Chauhan, P. S. B. Dev, I. Dubovyk, B. Dziewit, W. Flieger, K. Grzanka, J. Gluza, B. Karmakar, and S. Zieba, “Phenomenology of lepton masses and mixing with discrete flavor symmetries,” *Prog. Part. Nucl. Phys.* **138** (2024) 104126, [arXiv:2310.20681 \[hep-ph\]](https://arxiv.org/abs/2310.20681).
- [20] G.-J. Ding and S. F. King, “Neutrino mass and mixing with modular symmetry,” *Rept. Prog. Phys.* **87** no. 8, (2024) 084201, [arXiv:2311.09282 \[hep-ph\]](https://arxiv.org/abs/2311.09282).
- [21] G.-J. Ding and J. W. F. Valle, “The symmetry approach to quark and lepton masses and mixing,” *Phys. Rept.* **1109** (2025) 1–105, [arXiv:2402.16963 \[hep-ph\]](https://arxiv.org/abs/2402.16963).
- [22] **DUNE** Collaboration, R. Acciarri *et al.*, “Long-Baseline Neutrino Facility (LBNF) and Deep Underground Neutrino Experiment (DUNE): Conceptual Design Report, Volume 1: The LBNF and DUNE Projects,” [arXiv:1601.05471 \[physics.ins-det\]](https://arxiv.org/abs/1601.05471).
- [23] **DUNE** Collaboration, R. Acciarri *et al.*, “Long-Baseline Neutrino Facility (LBNF) and Deep Underground Neutrino Experiment (DUNE): Conceptual Design Report, Volume 4 The DUNE Detectors at LBNF,” [arXiv:1601.02984 \[physics.ins-det\]](https://arxiv.org/abs/1601.02984).
- [24] **DUNE** Collaboration, B. Abi *et al.*, “Experiment Simulation Configurations Approximating DUNE TDR,” [arXiv:2103.04797 \[hep-ex\]](https://arxiv.org/abs/2103.04797).
- [25] **Hyper-Kamiokande Proto-** Collaboration, K. Abe *et al.*, “Physics potential of a long-baseline neutrino oscillation experiment using a J-PARC neutrino beam and Hyper-Kamiokande,” *PTEP* **2015** (2015) 053C02, [arXiv:1502.05199 \[hep-ex\]](https://arxiv.org/abs/1502.05199).
- [26] **Hyper-Kamiokande** Collaboration, K. Abe *et al.*, “Physics potentials with the second Hyper-Kamiokande detector in Korea,” *PTEP* **2018** no. 6, (2018) 063C01, [arXiv:1611.06118 \[hep-ex\]](https://arxiv.org/abs/1611.06118).
- [27] W. Chao, “Quantum field theory approach to neutrino oscillations in dark matter and implications at JUNO,” [arXiv:2511.15494 \[hep-ph\]](https://arxiv.org/abs/2511.15494).
- [28] Y.-F. Li, A. Wang, Y. Xu, and J.-y. Zhu, “Terrestrial Matter Effects on Reactor Antineutrino Oscillations: Constant vs. Fluctuated Density Profiles,” [arXiv:2511.15702 \[hep-ph\]](https://arxiv.org/abs/2511.15702).
- [29] J. Huang and S. Zhou, “Probing unitarity violation of lepton flavor mixing matrix with reactor antineutrinos at JUNO and TAO,” [arXiv:2511.15525 \[hep-ph\]](https://arxiv.org/abs/2511.15525).
- [30] S.-F. Ge, C.-F. Kong, M. Lindner, and J. P. Pinheiro, “Neutrinoless Double Beta Decay in Light of JUNO First Data,” [arXiv:2511.15391 \[hep-ph\]](https://arxiv.org/abs/2511.15391).
- [31] Z.-z. Xing, “Divergence in tracing the flavors of astrophysical neutrinos: can JUNO help IceCube?,” [arXiv:2511.15127 \[hep-ph\]](https://arxiv.org/abs/2511.15127).

- [32] Z.-Q. Chen, G.-X. Fang, and Y.-L. Zhou, “Probing quark-lepton correlation in GUTs with high-precision neutrino measurements,” [arXiv:2511.16196 \[hep-ph\]](https://arxiv.org/abs/2511.16196).
- [33] G.-J. Ding, C.-C. Li, J.-N. Lu, and S. T. Petcov, “Discrete flavour and CP symmetries in light of JUNO and neutrino global fit,” [arXiv:2512.03809 \[hep-ph\]](https://arxiv.org/abs/2512.03809).
- [34] D. Borah, P. Das, and D. Dutta, “Neutrino texture-zeros after JUNO’s first results: Implications for long-baseline neutrino experiments,” [arXiv:2512.13587 \[hep-ph\]](https://arxiv.org/abs/2512.13587).
- [35] S. K. Nanda, M. Ricky Devi, C. Dash, R. N. Panda, and S. Patra, “An A_4 -Symmetric Double Seesaw for Neutrino Masses and Mixing in Light of JUNO results,” [arXiv:2512.24132 \[hep-ph\]](https://arxiv.org/abs/2512.24132).
- [36] E.-H. Shang, J.-N. Lu, G.-J. Ding, and S. F. King, “New modular fixed point models and their phenomenological implications for JUNO, T2HK and DUNE,” [arXiv:2601.09598 \[hep-ph\]](https://arxiv.org/abs/2601.09598).
- [37] D. Zhang, “Trimaximal Mixing Patterns Meet the First JUNO Result,” [arXiv:2511.15654 \[hep-ph\]](https://arxiv.org/abs/2511.15654).
- [38] X.-G. He, “Modified Tri-bimaximal neutrino mixing confront with JUNO θ_{12} measurement,” [arXiv:2511.15978 \[hep-ph\]](https://arxiv.org/abs/2511.15978).
- [39] W.-H. Jiang, R. Ouyang, and Y.-L. Zhou, “Modular TM₁ mixing in light of precision measurement in JUNO,” [arXiv:2511.16348 \[hep-ph\]](https://arxiv.org/abs/2511.16348).
- [40] G.-J. Ding, R. Kumar, N. Nath, R. Srivastava, and J. W. F. Valle, “Zooming in on ‘bi-large’ neutrino mixing with the first JUNO results,” [arXiv:2511.22689 \[hep-ph\]](https://arxiv.org/abs/2511.22689).
- [41] D. Dutta, S. Goswami, M. Kashav, and K. M. Patel, “Testing residual-symmetry-fixed columns of U_{PMNS} at DUNE and T2HK with initial JUNO constraints,” [arXiv:2601.18397 \[hep-ph\]](https://arxiv.org/abs/2601.18397).
- [42] P. F. Harrison and W. G. Scott, “mu - tau reflection symmetry in lepton mixing and neutrino oscillations,” *Phys. Lett. B* **547** (2002) 219–228, [arXiv:hep-ph/0210197](https://arxiv.org/abs/hep-ph/0210197).
- [43] P. Chen, G.-J. Ding, F. Gonzalez-Canales, and J. W. F. Valle, “Generalized $\mu - \tau$ reflection symmetry and leptonic CP violation,” *Phys. Lett. B* **753** (2016) 644–652, [arXiv:1512.01551 \[hep-ph\]](https://arxiv.org/abs/1512.01551).
- [44] N. Nath, Z.-z. Xing, and J. Zhang, “ $\mu - \tau$ Reflection Symmetry Embedded in Minimal Seesaw,” *Eur. Phys. J. C* **78** no. 4, (2018) 289, [arXiv:1801.09931 \[hep-ph\]](https://arxiv.org/abs/1801.09931).
- [45] K. Chakraborty, K. N. Deepthi, S. Goswami, A. S. Joshipura, and N. Nath, “Exploring partial $\mu - \tau$ reflection symmetry at DUNE and Hyper-Kamiokande,” *Phys. Rev. D* **98** no. 7, (2018) 075031, [arXiv:1804.02022 \[hep-ph\]](https://arxiv.org/abs/1804.02022).
- [46] N. Nath, “ $\mu - \tau$ reflection symmetry and its explicit breaking for leptogenesis in a minimal seesaw model,” *Mod. Phys. Lett. A* **34** no. 39, (2019) 1950329, [arXiv:1808.05062 \[hep-ph\]](https://arxiv.org/abs/1808.05062).
- [47] N. Nath, “Consequences of $\mu - \tau$ Reflection Symmetry at DUNE,” *Phys. Rev. D* **98** no. 7, (2018) 075015, [arXiv:1805.05823 \[hep-ph\]](https://arxiv.org/abs/1805.05823).

- [48] N. Nath, “Impact of RGE-induced $\mu - \tau$ reflection symmetry breaking on the effective Majorana neutrino mass in $0\nu\beta\beta$ decay,” *Phys. Rev. D* **99** no. 3, (2019) 035026, [arXiv:1810.07938 \[hep-ph\]](https://arxiv.org/abs/1810.07938).
- [49] J. Liao, N. Nath, T. Wang, and Y.-L. Zhou, “Nonstandard neutrino interactions and mu-tau reflection symmetry,” *Phys. Rev. D* **101** no. 9, (2020) 095036, [arXiv:1911.00213 \[hep-ph\]](https://arxiv.org/abs/1911.00213).
- [50] G.-y. Huang and N. Nath, “RGE-induced μ - τ symmetry breaking: an analysis of the latest T2K results,” *Eur. Phys. J. C* **80** no. 10, (2020) 914, [arXiv:2004.12391 \[hep-ph\]](https://arxiv.org/abs/2004.12391).
- [51] M. J. S. Yang, “Interplay between exact μ - τ reflection symmetries, four-zero texture and universal texture,” *Phys. Lett. B* **806** (2020) 135483, [arXiv:2002.09152 \[hep-ph\]](https://arxiv.org/abs/2002.09152).
- [52] Z.-h. Zhao, “Combinations of the μ - τ reflection symmetry and texture zeros in the Dirac neutrino mass matrix of the seesaw model,” *Eur. Phys. J. Plus* **138** no. 11, (2023) 1055.
- [53] Y. Shao and Z.-h. Zhao, “Low scale leptogenesis under neutrino $\mu - \tau$ reflection symmetry,” *Phys. Rev. D* **111** no. 3, (2025) 035011, [arXiv:2409.04089 \[hep-ph\]](https://arxiv.org/abs/2409.04089).
- [54] M. J. S. Yang, “Almost general analysis of μ - τ reflection symmetry perturbed by charged leptons and its testability by DUNE and T2HK,” *Nucl. Phys. B* **1018** (2025) 117092, [arXiv:2504.00365 \[hep-ph\]](https://arxiv.org/abs/2504.00365).
- [55] K. S. Babu, E. Ma, and J. W. F. Valle, “Underlying $A(4)$ symmetry for the neutrino mass matrix and the quark mixing matrix,” *Phys. Lett. B* **552** (2003) 207–213, [arXiv:hep-ph/0206292](https://arxiv.org/abs/hep-ph/0206292).
- [56] S.-L. Chen, M. Frigerio, and E. Ma, “Hybrid seesaw neutrino masses with $A(4)$ family symmetry,” *Nucl. Phys. B* **724** (2005) 423–431, [arXiv:hep-ph/0504181](https://arxiv.org/abs/hep-ph/0504181).
- [57] G. Altarelli and F. Feruglio, “Tri-bimaximal neutrino mixing, $A(4)$ and the modular symmetry,” *Nucl. Phys. B* **741** (2006) 215–235, [arXiv:hep-ph/0512103](https://arxiv.org/abs/hep-ph/0512103).
- [58] D. Borah and B. Karmakar, “ A_4 flavour model for Dirac neutrinos: Type I and inverse seesaw,” *Phys. Lett. B* **780** (2018) 461–470, [arXiv:1712.06407 \[hep-ph\]](https://arxiv.org/abs/1712.06407).
- [59] S. Centelles Chuliá, R. Srivastava, and J. W. F. Valle, “Generalized Bottom-Tau unification, neutrino oscillations and dark matter: predictions from a lepton quarticity flavor approach,” *Phys. Lett. B* **773** (2017) 26–33, [arXiv:1706.00210 \[hep-ph\]](https://arxiv.org/abs/1706.00210).
- [60] D. Borah and B. Karmakar, “Linear seesaw for Dirac neutrinos with A_4 flavour symmetry,” *Phys. Lett. B* **789** (2019) 59–70, [arXiv:1806.10685 \[hep-ph\]](https://arxiv.org/abs/1806.10685).
- [61] G.-J. Ding, J.-N. Lu, and J. W. F. Valle, “Trimaximal neutrino mixing from scotogenic A_4 family symmetry,” *Phys. Lett. B* **815** (2021) 136122, [arXiv:2009.04750 \[hep-ph\]](https://arxiv.org/abs/2009.04750). [Erratum: *Phys.Lett.B* 845, 138151 (2023)].
- [62] M. Ricky Devi and K. Bora, “Linking resonant leptogenesis with dynamics of the inverse seesaw theory with A_4 flavor symmetry,” [arXiv:2304.13546 \[hep-ph\]](https://arxiv.org/abs/2304.13546).
- [63] S. Centelles Chuliá, R. Kumar, O. Popov, and R. Srivastava, “Neutrino mass sum rules from modular A_4 symmetry,” *Phys. Rev. D* **109** no. 3, (2024) 035016, [arXiv:2308.08981 \[hep-ph\]](https://arxiv.org/abs/2308.08981).

- [64] R. Kumar, P. Mishra, M. K. Behera, R. Mohanta, and R. Srivastava, “Predictions from scoto-seesaw with A_4 modular symmetry,” *Phys. Lett. B* **853** (2024) 138635, [arXiv:2310.02363 \[hep-ph\]](https://arxiv.org/abs/2310.02363).
- [65] L. Singh, M. Kashav, and S. Verma, “Minimal type-I Dirac seesaw and leptogenesis under A_4 modular invariance,” *Nucl. Phys. B* **1007** (2024) 116666, [arXiv:2405.07165 \[hep-ph\]](https://arxiv.org/abs/2405.07165).
- [66] R. Kumar, N. Nath, and R. Srivastava, “Cutting the scotogenic loop: adding flavor to dark matter,” *JHEP* **12** (2024) 036, [arXiv:2406.00188 \[hep-ph\]](https://arxiv.org/abs/2406.00188).
- [67] T. Nomura and H. Okada, “Type-II seesaw of a non-holomorphic modular A_4 symmetry,” *Phys. Lett. B* **868** (2025) 139763, [arXiv:2408.01143 \[hep-ph\]](https://arxiv.org/abs/2408.01143).
- [68] A. Palavrić, “Discrete leptonic flavor symmetries: UV mediators and phenomenology,” *Phys. Rev. D* **110** no. 11, (2024) 115025, [arXiv:2408.16044 \[hep-ph\]](https://arxiv.org/abs/2408.16044).
- [69] A. Moreno-Sánchez and A. Palavrić, “Leptonic flavor from a modular A_4 symmetry: UV mediators and SMEFT realizations,” *Phys. Rev. D* **112** no. 7, (2025) 075002, [arXiv:2505.01535 \[hep-ph\]](https://arxiv.org/abs/2505.01535).
- [70] R. Kumar, N. Nath, R. Srivastava, and S. Yadav, “Dirac Scoto inverse-seesaw from A_4 flavor symmetry,” *JHEP* **10** (2025) 088, [arXiv:2505.01407 \[hep-ph\]](https://arxiv.org/abs/2505.01407).
- [71] R. Kumar, H. K. Prajapati, R. Srivastava, and S. Yadav, “Flavor imprints on novel low mass dark matter,” *JHEP* **11** (2025) 094, [arXiv:2510.02972 \[hep-ph\]](https://arxiv.org/abs/2510.02972).
- [72] S. Centelles Chuliá and R. Kumar, “Minimal A_4 Type-II Seesaw Realization of Testable Neutrino Mass Sum Rules,” [arXiv:2512.22343 \[hep-ph\]](https://arxiv.org/abs/2512.22343).
- [73] H. Ishimori, T. Kobayashi, H. Ohki, Y. Shimizu, H. Okada, and M. Tanimoto, “Non-Abelian Discrete Symmetries in Particle Physics,” *Prog. Theor. Phys. Suppl.* **183** (2010) 1–163, [arXiv:1003.3552 \[hep-th\]](https://arxiv.org/abs/1003.3552).
- [74] J. Schechter and J. W. F. Valle, “Neutrino Masses in $SU(2) \times U(1)$ Theories,” *Phys. Rev. D* **22** (1980) 2227.
- [75] M. Magg and C. Wetterich, “Neutrino Mass Problem and Gauge Hierarchy,” *Phys. Lett. B* **94** (1980) 61–64.
- [76] T. P. Cheng and L.-F. Li, “Neutrino Masses, Mixings and Oscillations in $SU(2) \times U(1)$ Models of Electroweak Interactions,” *Phys. Rev. D* **22** (1980) 2860.
- [77] R. N. Mohapatra and G. Senjanovic, “Neutrino Masses and Mixings in Gauge Models with Spontaneous Parity Violation,” *Phys. Rev. D* **23** (1981) 165.
- [78] A. Degee, I. P. Ivanov, and V. Keus, “Geometric minimization of highly symmetric potentials,” *JHEP* **02** (2013) 125, [arXiv:1211.4989 \[hep-ph\]](https://arxiv.org/abs/1211.4989).
- [79] S. Carrolo, J. C. Romao, and J. P. Silva, “Conditions for global minimum in the A_4 symmetric 3HDM,” *Eur. Phys. J. C* **82** no. 8, (2022) 749, [arXiv:2207.02928 \[hep-ph\]](https://arxiv.org/abs/2207.02928).
- [80] P. F. de Salas, D. V. Forero, S. Gariazzo, P. Martínez-Miravé, O. Mena, C. A. Ternes, M. Tórtola, and J. W. F. Valle, “2020 global reassessment of the neutrino oscillation picture,” *JHEP* **02** (2021) 071, [arXiv:2006.11237 \[hep-ph\]](https://arxiv.org/abs/2006.11237).

[81] W. Rodejohann and J. W. F. Valle, “Symmetrical Parametrizations of the Lepton Mixing Matrix,” *Phys. Rev. D* **84** (2011) 073011, [arXiv:1108.3484 \[hep-ph\]](https://arxiv.org/abs/1108.3484).